December 1974 LRP 88/74

GENERATION OF MONOCHROMATIC ELECTROSTATIC WAVES OF LARGE AMPLITUDES IN A BOUNDED BEAM-PLASMA SYSTEM

M. Bitter and P.J. Paris

Centre de Recherches en Physique des Plasmas

ECOLE POLYTECHNIQUE FEDERALE DE LAUSANNE

November 1974 LRP 88/74

GENERATION OF MONOCHROMATIC ELECTROSTATIC WAVES OF LARGE AMPLITUDES IN A BOUNDED BEAM-PLASMA SYSTEM

M. Bitter and P.J. Paris

INTRODUCTION

The propagation of single electrostatic waves of large amplitudes in a plasma gives rise to a number of non-linear effects, which have found considerable interest in the last few years. These effects are the coupling and parametric amplification of waves /1-3/ and the trapping of particles /4-8/, which leads to a periodic exchange of energy between the wave and the trapped particles.

The generation of large amplitude electrostatic waves by external excitation from an antenna is difficult in some circumstances due to a weak coupling factor /9/. The possibility of exciting waves by the interaction of an electron beam with the plasma /6-8, 10-15/ offers certain advantages in this respect.

This is a report on an experimental study of the interaction of an electron beam with a bounded plasma. Monochromatic electrostatic waves of large amplitudes are excited by an amplification of the beam modes in a resonance cavity. Non-linear effects as the generation of harmonics and sidebands have been observed.

I. EXPERIMENT

1. The device and the experimental parameters

The experiments have been performed in a stationary argon plasma which was produced in a hot cathode glow discharge, Fig. 1. Electrons emitted from an indirectly heated cathode of 5 cm diameter are accelerated by a potential difference between the negatively biased cathode and an earthed coarse (80% transmission) grid 32 mm in front of the cathode and produce a plasma by ionizing collisions with the neutral gas at pressures of about 5×10^{-4} mn Hg*.

The plasma can be confined within a column of the cathode diameter by a homogeneous magnetic field, whose strength is variable up to 3 kgauss. Without magnetic field it extends over the whole volume of the glass tube, which has a diameter of 15 cm. The length of the column is variable up to 85 cm by a longitudinally movable anode, which was usually earthed or floating.

Fig. 1 shows the longitudinal and radial density profiles of the plasma for cases with and without magnetic field. The profiles are considerably smoother without magnetic field.

The plasma diagnostics are performed by use of longitudinally and radially movable Langmuir probes and by measuring the propagation characteristics of Bernstein waves / 16 /. This method gives rather precise results on the electron temperature and plasma density and allows a calibration of the Langmuir probe measurements.

---

*The plasma is weakly ionized. The ratio of primary to secondary electrons is about 5 %. Electron neutral collisions are dominant, but as the collision frequency ($\nu_{coll.} \approx$ 15 MHz) is small compared to the electron plasma frequency ($\nu_p \approx$ 500 MHz), they do not affect the growth rate of the instabilities /11 /.

The range of our experimental parameters is given in the diagram of Fig. 2, which shows the relations between the discharge voltage V_D, the plasma density (measured by the ion saturation current I_{sat}^{ion} taken from a Langmuir probe) and the discharge current I_D, for a given neutral gas pressure and different values of the magnetic field. (Gas pressure and magnetic field are the independent parameters). The plasma density increases proportional to I_D with a constant of proportionality, which is dependent on B. For a given discharge current I_D the discharge voltage decreases with increasing magnetic field. This is because the number of plasma electrons, which carry the discharge current together with the primary electrons, increases through the reduction of diffusion losses. Therefore V_D tends towards a lower limit at high magnetic fields, where diffusion losses are negligible.

A calibration of the measured ion saturation current is easily obtained from the density measurements with Bernstein waves given in Table 1.

I_D [A]	ν_{ce} [x 10^8 Hz]	ν_p [x 10^8 Hz]
.100	3.40	3.5
.135	2.95	3.8
.165	2.20	4.3
.200	1.90	4.4
.242	1.30	4.6
.270	1.00	4.7

Table 1

(The magnetic field and the plasma density are given in units of the electron cyclotron (ν_{ce}) and electron plasma frequency (ν_p), respectively).

2. The observed power spectra

Investigating the noise power spectra of the plasma for different experimental parameters we found sharp intensity maxima, which were 20 to 60 dB above the noise level. These maxima occured at the harmonics of certain frequencies, which were well removed from the characteristic frequencies (ν_{ce}, ν_p) of the plasma, and were surrounded by a number of equidistant satellite lines in some cases (see Figs. 3,4,9,10).

The spectra in the Figures have been measured by means of two Rhode & Schwarz receivers, type USVV BN 1522 (freq. range: 30 - 480 MHz) and type USVB BN 15241 (freq. range: .17 - 4.4 GHz), with resolutions of 20 kHz and .4 MHz, respectively, analyzing the r.f. signals taken from a Langmuir probe, the anode or the cathode. Type USVB is a swept frequency receiver yielding two output signals, which are proportional to the frequency and the measured intensity. These outputs have been used to drive the coordinates of a xy-recorder.

The origin of the oscillations is found in the cathode grid region, which acts as a resonance cavity for waves, whose wavelengths are half an integer fraction of the cathode grid distance, i.e. $\lambda = \frac{64}{n}$ [mm] (see Fig. 5)*.

These experimental results suggest the following interpretation: The oscillations are electrostatic waves, which are excited by the interaction of the fast primary electrons with the plasma. Multiple reflection at the grid and cathode lead to an amplification and to the formation of standing waves in the cathode grid region, if the wavelength satisfies the resonance condition. In this case the amplification is so strong that waves at the higher harmonics are generated by non-linear effects. As the grid is not a perfect

---

*The measurements shown in Fig. 5 have been carried out on the anode side of the grid. The wavelengths belonging to the lower frequencies with $\omega \approx \omega_p$ show considerable spatial variation obviously due to the density gradient in the plasma, whereas the wavelengths at the higher harmonics, which are well above ω_p, are constant.

We have also measured the spatial oscillations in the cathode grid region, where we found half the wavelength.

reflector a part of the energy is always transmitted into the anode grid region. The transmitted wave is a propagating wave.

This interpretation requires a detailed consideration of the dispersion characteristics of the plasma, the qualities of the electron beam and the nature of the beam plasma interaction. This aspects are discussed in the following sections.

II. THEORY

1. Dispersion relations for electrostatic waves in a cylindrical bounded plasma

The eigenvalue problem yielding the dispersion relations for waves propagating in a finite plasma involves certain conditions for the electric and magnetic fields of the waves, which depend on the specific geometry and nature of the boundaries.

The dispersion relations for electrostatic waves in a cylindrically bounded, infinitely long, cold plasma of homogeneous density have been calculated by Trivelpiece and Gould / 17 /. They showed that there exists an infinite number of solutions belonging to a set of orthogonal eigenfunctions $\phi_{n\nu}$ for the electrostatic wave potential. The $\phi_{n\nu}$ are expressed in terms of Bessel-functions, which satisfy the specific boundary conditions. Eq.(1) represents the dispersion relation for the case of a plasma column of radius a, which is surrounded by a dielectricum with a dielectric constant K_e and an outer conducting wall of inner radius b.

$$(1)\quad \varepsilon_1 k_\perp a \frac{J_n'(k_\perp a)}{J_n(k_\perp a)} + n\varepsilon_2 = K_e k_{11} a \frac{I_n'(k_{11}a) K_n(k_{11}b) - I_n(k_{11}b) K_n'(k_{11}a)}{I_n(k_{11}a) K_n(k_{11}b) - I_n(k_{11}b) K_n(k_{11}a)}$$

with $$k_\perp^2 = - k_{II}^2 \frac{\varepsilon_3}{\varepsilon_1}$$

($k_\perp$, k_{II} are the axial and radial wave numbers, respectively).

$$\varepsilon_1 = 1 - \frac{\omega_p^2}{\omega^2 - \omega_c^2}$$

$$\varepsilon_2 = \frac{- \omega_p^2 \omega_c}{\omega (\omega^2 - \omega_c^2)}$$

$$\varepsilon_3 = 1 - \frac{\omega_p^2}{\omega^2}$$

(The ions are considered as neutralizing background). Standard notation is used for the Bessel functions.

The solutions are classified according to their angular (n = 1,2,3....) and radial (ν = 1,2,3..., ν-th zero of the n-th order Bessel function) quantum numbers.

Several authors have calculated dispersion relations including the effects of an inhomogeneous density profile and a finite electron temperature. The calculations consider parabolic / 18 / or measured / 19 / density profiles and account for the temperature introducing the Landau expressions for $\underline{\underline{\varepsilon}}$.

The shape of the density profile has only little effect on the dispersion. This is because the density profile enters into the eigenvalues only through an integral expression / 11 /.

A finite electron temperature causes a shift of the frequencies towards higher values and introduces Landau damping. This is especially important

for short wavelengths of the order of a few Debye-lengths, but does not affect the low frequency long wavelength oscillations.

Fig. 6 shows the dispersion curves for the low order radial modes with no angular dependence computed from eq. 1 for typical experimental conditions $\left(K_e = 1, \frac{\omega_c}{\omega_p} = .58, \frac{b}{a} = 3\right)$ *

It should be noticed that the lowest order mode (n, ν = 0) saturates at $\omega = \frac{\omega_p}{\sqrt{1+K_e}}$ and the higher order modes (n = 0, $\nu \gg 1$) saturate at ω_{ce} with $k_{\parallel}$ approaching infinity. Therefore the higher order modes vanish with the magnetic field.

2. Interaction of the slow space charge wave of an electron beam with the plasma /10,11/.

This type of interaction is described by eq. 2

(2) $$\varepsilon_p(\omega, k) = \frac{\omega_{pb}^2}{(\omega - k v_0)^2}$$ **

---

* There is no appreciable change of the dispersion curves for $\frac{b}{a} \geq 3$. This means that the conditions imposed on the electrostatic wave potential by the second boundary need not be considered in these cases.

** Eq.2 holds for a cold beam and identical density profiles of the beam and the plasma. If the density profiles are different (and inhomogeneous), the eigenmodes of the beam-plasma system are coupled and the RHS of eq.2 is replaced by a sum of coupling terms. However, the unstable modes of the system are still described by eq.2, if ω_{pb}^2 is multiplied by an appropriate reduction factor / 11 /.

where

$\varepsilon_p(\omega, k)$ is the dielectric of the plasma

ω_{pb} the plasma frequency of the electron beam

v_o the velocity of the beam

Under the assumption of a weak beam ($\frac{\omega_{pb}^2}{\omega_p^2} << 1$) one obtains two types of solutions for eq. 2:

1. The normal plasma modes, for instance the Trivelpiece-Gould modes in the case of a bounded plasma

   (for $\omega \neq k\ v_o$, off-resonance modes)

and

2. The beam modes

   (for $\omega \approx k\ v_o$, resonant modes)

Eq.2 yields two complex solutions describing a damped and a growing beam mode, if the dielectric of the plasma is negative ($\varepsilon_p(\omega, K) < 0$). As this condition is fullfilled for (ω, k)- values below the plasma dispersion curve, an unstable (growing) beam mode can exist only, if the velocity of the beam is smaller than a critical velocity v_c , which is given by the slope of the dispersion curve for ω, $k \longrightarrow 0$ (see Fig. 5). This is the threshold criterium for unstable waves.

For a rough estimate of the critical velocity we take the slope of the ground mode for a plasma filled wave guide, which can be described by a

simple analytic expression. This yields

(3) $$v_0 \leq \frac{\omega_p a}{p_{00}}$$

where $p_{00} = 2.4$ is the first zero of the zero order Bessel function.

The growth rate assumes the maximum value

$$\omega_{i\,max} \sim \left(\frac{\omega_{pb}}{\omega_p}\right)^{2/3} \omega_p$$

for $\varepsilon_p(\omega,k) \approx 0$, i.e. for ω, k - values near the intersection points of beam - and plasma modes in Fig. 5 (Synchronism of a beam mode with a plasma mode).

The growth rate is considerably reduced, if the beam electrons have a finite velocity spread. This means that synchronism is a necessary condition for the excitation of an instability of an appreciable growth rate in the case of a hot beam.

The cold beam model is a valid approximation, if the following criterium is satisfied.

(4) $$\frac{\Delta v}{v_0} << \left(\frac{\omega_{pb}}{\omega_p}\right)^{2/3}$$

where Δv is the velocity spread of the beam electrons (The beam has to be considered as hot, if inequality (4) is reversed).

III. DISCUSSION

1. The dominant lines of the spectra

Applying criterium (4) to our experimental cases we find that the cold beam model is a reasonable approach for the case without magnetic field, whereas the cases with magnetic field fall in between the validity ranges for the cold and hot beam models.

This is because the discharge voltage V_D, which yields the main contribution to the acceleration of the beam electrons, decreases and the plasma density (ω_p^2) increases with the magnetic field (see diagram with the experimental parameters in Fig. 2). Moreover, the radial variation of the plasma potential, which is the other part of the acceleration voltage, causes a spread of the beam velocity ("pseudo temperature") / 19 /, which is relatively larger with magnetic field because of the steeper gradient (see Fig. 1).

However, apart from criterium (4) there is a sensitive experimental possibility to decide whether the beam is to be considered as hot or cold. This is a measurement of the dispersion characteristics of the beam-plasma system / 20 /. For the case of a weak hot beam the real part of the dispersion of the compound (beam-plasma) system must be the same as for the plasma alone. The only effect of the beam is to change certain originally damped plasma modes into slightly growing waves. On the other hand, the dispersion is significantly changed by the presence of a cold beam / 21 /.

We have measured the dispersion curve by means of an interferometer circuit /9, 18,19/ using two Langmuir probes as transmitter and receiver of CW r.f. signals, Fig. 7 . Though the precision of the wavelength measurements at lower frequencies is affected by the density gradients, one can clearly see a bending over from the plasma modes at low frequencies to the beam modes at higher frequencies. This indicates that the beam cannot be considered as hot /20,21/.

In the following we will not try to identify the spontaneous excited waves as special Trivelpiece-Gould modes, for the following reason:

> The condition of synchronism, which implies that the excited mode is a plasma mode, is not a strict one both for the reasons given above (cold or hot beam) and because due to the mechanism of amplification by reflection in the cavity the wave with the largest amplitude is not necessarily the fastest growing one in the sense of the usual theory.

Instead of this we will apply some general criteria of the theory to our experiments. These are:

1. The threshold criterium, eq.(3)

2. The lowest excited frequency ω_o must be smaller than the saturation frequency $\omega_p / \sqrt{1 + K_e}$ of the plasma ground mode.

3. The waves excited at the harmonics of ω_o should follow a straight dispersion line, the slope of which is given by the beam velocity.

We have checked the threshold criterium by the series of measurements shown in Fig. 8. The spectra have been taken for a fixed discharge current and different values of the magnetic field.

These spectra are well understood with the aid of Fig. 2. The threshold is passed for a certain value of the magnetic field (ν_{ce} = 250 MHz, in Fig. 8), as the plasma density increases and the discharge voltage V_D (beam velocity !) decreases with increasing magnetic field for a given discharge current I_D.

Increasing the magnetic field beyond the threshold value causes a shift of the intensity maxima towards lower frequencies. This can be considered as a confirmation of two assumptions:

a) The excited cavity modes are beam modes with $\omega = k\ v_o$. Thus, the frequency decreases with the beam velocity, as the k-value is fixed by the resonance condition of the cavity.

b) These beam modes are not synchroneous with Trivelpiece-Gould modes, because the saturation frequencies (whereabout the points of intersection with the beam modes are) are rised up
   - for all modes,
   - for the higher order radial modes due to the increase of magnetic field,
   - for the ground mode due to the increase of plasma density (see Fig. 6).

The second criterium mentioned above was fullfilled for all observed spectra with unstable waves.

With regard to the third criterium we have found that the waves belonging to the harmonics followed a straight dispersion line. The slope of this line was found to be equal to the beam velocity in the case without magnetic field, but it was slightly higher ($\approx$ 20 %) than the beam velocity in the other cases. The beam velocity was calculated from the potential difference between plasma and cathode. We think that the discrepancy could be explained, if one accounts for a finite temperature of the beam, which changes the phase velocity of the

waves supported by the beam by about the thermal velocity spread*. The velocity spread of the beam is larger with than without magnetic field due to the pseudotemperature introduced by the radial variation of the plasma potential. Measurements of the beam velocity distribution have shown a temperature spread of about 1 eV /16/. This gives for typical discharge voltages of 20 - 30 volts values of about 20 % for $\frac{\Delta v}{v_o}$.

2. The sidebands

In some cases we have observed two or even more (up to 10) equidistant sidebands around the main peaks of the frequency spectra (see Figs. 9-12).

These sidebands are not cavity modes as the modes belonging to the main peaks of the spectrum, but are generated between grid and anode further along the plasma column. This has been proved by varying the anode grid distance (see Fig.11). The sidebands disappear in the background noise, if the grid distance is below a certain minimum value (30 cm, in Fig.11) and grow in amplitude, if the distance is increased beyond this value, whereas the amplitude of the main peak does not change appreciably.

---

*The difference of the slope cannot be caused by effects like the finite boundaries or a drift of the plasma against the beam /22/. The effect of the boundaries on the beam modes (at high frequencies) is only a parallel shift of the dispersion line, but not a change of the slope. A drift of the main plasma is unimportant, because, as the modes are carried by the beam, there matters only the velocity of the beam relative to the laboratory.

There are two physical processes, which may cause these sidebands:

1. The trapping of beam electrons in the potential wells of the large amplitude (cavity) wave / 4-8 /. This leads to a periodic exchange of energy between the trapped particles and the wave, i.e. a modulation of the wave amplitude at the bounce frequency

$$\omega_b = \left(\frac{e}{m} E k\right)^{1/2}$$

where k and E are the wave number and electric field of the wave, respectively. Higher order sidebands at frequencies $\omega_n = \omega_o \pm n\omega_b$ may then be excited by a mechanism described by Kruer et al. / 23 /, where the trapped particles act as a bunched beam*.

2. Three wave coupling. This process is most probable for the resonant beam modes, as the conservation laws

$$\omega_o = \omega_1 + \omega_2 \,, \quad k_o = k_1 + k_2$$

are easily fullfilled because of the linearity of their dispersion. The excitation of sidebands (also of higher orders) has been explained by Chang et al. as due to this process assuming a remixing of waves, which are amplified by a process similar to the parametric amplification of waves in a plasma with negative energy waves / 24 /.

---

*Another explanation for the generation of sidebands has been given by de Neef et al. / 25 /, who calculated the modulation of the wave, that has trapped the beam, by a testwave at a neighbouring frequency.

IV. CONCLUSION

Monochromatic electrostatic waves with amplitudes of 20 - 60 dB above the noise level have been generated by the interaction of an electron beam with a bounded plasma. These waves have been identified as resonant beam modes, which are amplified by multiple reflection within a cavity (cathode grid region of the discharge). The existance of a threshold for the excitation of the waves has been proved experimentally by varying the beam velocity and the plasma density.

Non-linear effects as the generation of harmonics and sidebands have been observed. The sidebands may be generated by two non-linear processes, which are both possible in our machine, i.e. a trapping of the beam electrons or a coupling of the linearly dispersed beam modes. Further experiments including an analysis of the velocity distribution of the beam electrons are planed, in order to decide which process is dominant.

The cathode-grid distance of the discharge was a fixed parameter in the present experimental configuration. It may be desirable for future experiments to have this parameter variable, because it allows

a) a selection of the frequency and wavelength of the excited large amplitude electrostatic wave, which may be useful for a parametric experiment

and

b) a stabilization of the system, by shortening the cathode grid distance to a value such that the frequency of the lowest beam mode, whose wavelength fullfills the resonance condition of the cavity, is above the saturation frequency of the ground mode of the plasma.

The first process is only possible, if the length of the machine is greater than a length $\lambda_{osc.}$, which is characteristic for one oscillation of the trapped electrons.

This yields the criterium

$$L > \lambda_{osc.} = v_o \tau$$

where L is the machine length, $\tau = \frac{1}{\nu_b}$ the period of the oscillation and v_o the velocity of the beam electrons.

If we calculate $\lambda_{osc.}$ for our experiment taking $v_o \approx 4 \times 10^8$ [cm/s] and ν_b = 20 MHz, i.e. the frequency separation of the first sideband from the main peak in Fig.9, we obtain $\lambda_{osc.} \approx$ 20 cm. Thus particle trapping is a possible process.

We have also tried to generate sidebands by launching a wave at a frequency, which was close to the frequency of the main (cavity) wave /15,25,26/. This usually led to the appearance of two additional lines in the spectrum, which were symmetrically placed around the main peak, provided that the anode grid distance was greater than a certain length (about 30 cm). For smaller distances we found only the line of the launched wave. More than two additional lines have been observed only, if the original spectrum showed already satellites (see Fig. 12).

ACKNOWLEDGEMENT

We would like to thank Mr. R. Gruber and Mr. Gno for the computation of the dispersion diagram. The helpful discussions with Drs. Nguyen The Hung, F. Troyon, Mr. M.Q. Tran and Prof. E.S. Weibel are also gratefully acknowledged.

REFERENCES

1. W. Carr, D. Boyd, H. Lin, G. Schmidt and M. Seidl, Phys.Rev.Lett. 28, 662 (1972)

2. J. Chang, M. Raether and S. Tanaka, Phys.Rev.Lett. 27, 1263 (1971)

3. M. Porkolab, MATT-1049, June 1974

4. T.M. O'Neil, J.H. Winfrey, J.H. Malmberg, Phys.Fluids 14, 1204 (1971)

5. T.M. O'Neil and J.H. Winfrey, Phys.Fluids 15, 1514 (1972)

6. K.W. Gentle and C.W. Roberson, Phys.Fluids 14, 2780 (1971)

7. J.H.A. Van Wakeren and J.H. Hopman, Phys.Rev.Lett. 28, 295 (1972)

8. K.W. Gentle and J. Lohr, Phys.Fluids 16, 1464 (1973)

9. R.N. Franklin, S.M. Hamberger, G. Lampis and G.J. Smith, Culham Laboratory Report, CLM-R 131

10. R.J. Briggs, "Electron-Beam Interaction with Plasmas", Research Monograph, No 29 (1964), M.I.T. Press Cambridge, Massachusetts

11. R.J. Briggs, "Advances in Plasma Physics" Vol. 4, p. 43 (1971), edited by A. Simon and W.B. Thompson, J.Wiley & Sons, Inc., New York

12. M.V. Nezlin, G.I. Sapozhnikov and A.M. Solntsev, Soviet Physics, JETP 23, 2, 232, (1966)

13. T.A. Hall, Plasma Physics, Vol. 14, 667 (1972)

14. M. Seidl and P. Sunka, Nucl.Fusion 7, 237 (1967)

15. C.W. Roberson and J. Fukai, J.Appl.Phys. 45, 2489 (1974)

16. M.Bitter and P.J. Paris, LRP 82/74

17. A.W. Trivelpiece and R.W. Gould, J.Appl.Phys. 30, 11, 1784 (1959)

18. P.J. Barrett and H.G. Jones, Plasma Physics, 10, 911 (1968)

19. J.H. Malmberg and C.B. Wharton, Phys.Fluids 13, 2600 (1969)

20. K.W. Gentle and C.W. Roberson, Phys.Rev.Lett. 26, 226 (1971)

21. T.M. O'Neil, J.H. Malmberg, Phys.Fluids 11, 1754 (1968)

22. T.A. Hall, V European Conference on Controlled Fusion and Plasma Physics, Grenoble 1972

23. W.L. Kruer, J.M. Dawson and R.N. Sudan, Phys.Rev.Lett. 23, 838 (1969)

24. R. Goldman, R. Davidson, A. Hasegawa, Phys.Fluids 6, 1247 (1969)

25. C.P. De Neef, J.H. Malmberg and T.M. O'Neil, Phys.Rev. 30, 1032 (1973)

26. W. Carr, D. Bollinger, D. Boyd, H. Liu and M. Seidl, Phys.Rev.Lett. 30, 84 (1972)

FIGURE CAPTIONS

Fig. 1 Experimental device. Longitudinal (a) and radial (b) density profiles with and without magnetic field for a fixed discharge current (I_D = 300 mA). The density has been measured by the ion saturation current taken from a Langmuir probe.

Fig. 2 Diagram showing the variation of the discharge voltage V_D (dashed lines) and plasma density measured by the ion saturation current I_{ion}^{sat} from a Langmuir probe (solid lines) with the discharge current I_D for different values of the magnetic field and a gas pressure of 5×10^{-4} mm Hg.

Fig. 3 Spectrum obtained for a discharge current I_D of 300 mA and zero magnetic field ($\nu_{ce} = 0$). (The intensity is measured on a linear scale for all spectra).

Fig. 4 Spectrum obtained for I_D = 310 mA and ν_{ce} = 270 MHz.

Fig. 5 Figs.(a) and (b) show the spatial oscillations for the spectral lines in Figs. 3 and 4, respectively. The measurements have been obtained from the interference of the electric fields of the wave and of a capacitively coupled signal from the cathode /16/.

Fig. 6 Dispersion curves for the low order radial modes with no angular dependence computed from equ.1 for $K_e = 1$, $\frac{\nu_{ce}}{\nu_p} = .58$, $\frac{b}{a} = 3$. The slope of the beam modes $(\frac{v_o}{\omega_p a})$ has been calculated taking $v_o = 4 \times 10^8$ cm/s, $\nu_p = 4.5 \times 10^8$ MHz, a = 2.5 cm.

Fig. 7 Measured points of the dispersion relation of the beam plasma system for I_D = 280 mA, V_D = 27 volts, ν_{ce} = 250 MHz, $\nu_p \approx 425$ MHz.

The experimental points are close to the theoretical dispersion curve for the ground mode of the plasma at lower frequencies and follow a straight line, which is about the dispersion line for the beam modes, at higher frequencies. (The theoretical dispersion curve for the ground mode of the plasma has been computed from equ.1 approximating the radial density profile by a homogeneous profile of a radius a = 1.1 cm).

Fig. 8 Spectra obtained for a constant discharge current (I_D = 200 mA) and different values of the magnetic field.

Figs. 9-10 Spectra with equidistant sidebands around the dominant lines, which correspond to the resonant (cavity) modes.

Fig. 11 Spectra obtained for different values (10 cm, 30 cm, 55 cm) of the anode grid distance.

Fig. 12 Generation of sidebands by exciting a wave at a frequency (242 MHz), which is close to the frequency (254 MHz) of the main (cavity) mode. The wave has been launched from the cathode. (Original spectrum (a); modified spectrum (b)).

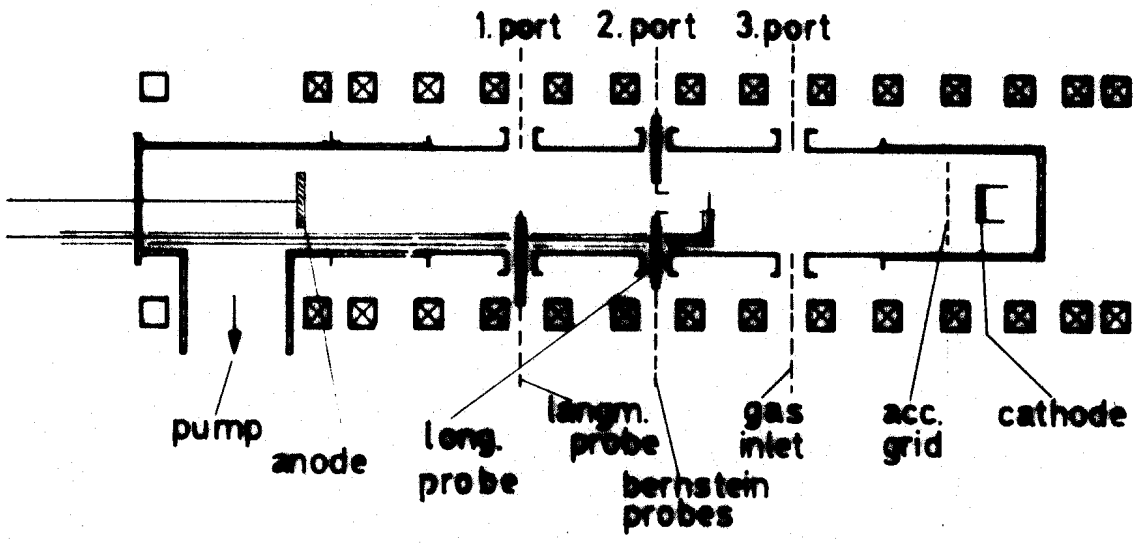
1. port
2. port
3. port
pump
anode
long. probe
langm. probe
bernstein probes
gas inlet
acc. grid
cathode

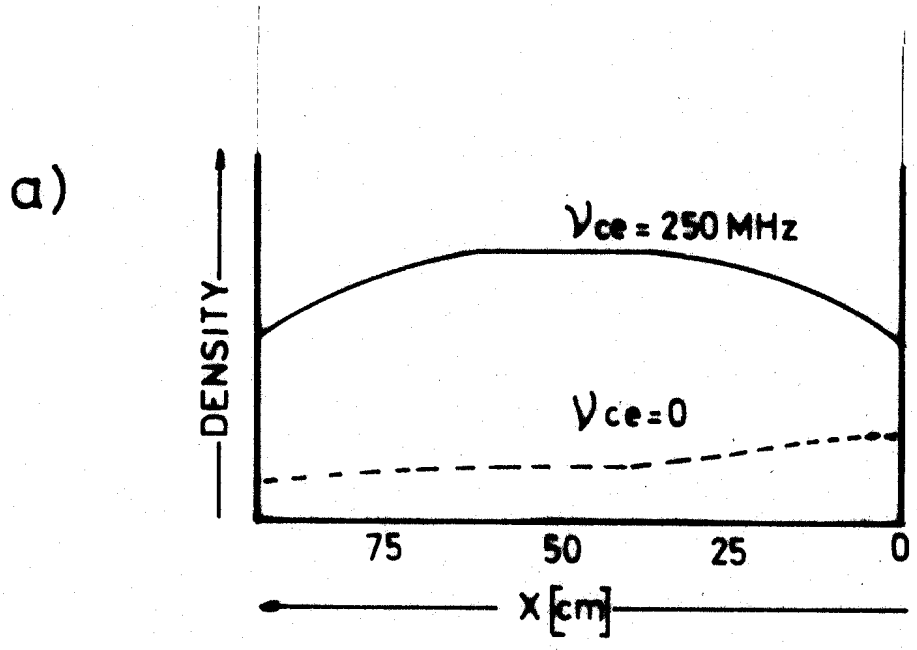
a)
DENSITY
ν_{ce} = 250 MHz
ν_{ce}=0
75
50
25
0
X [cm]

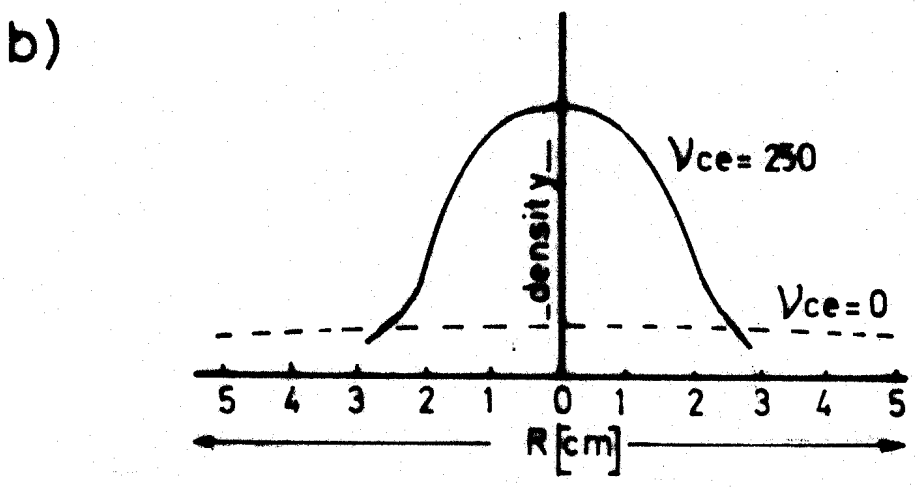
b)
density
ν_{ce}= 250
ν_{ce}=0
5 4 3 2 1 0 1 2 3 4 5
R [cm]

Fig. 1

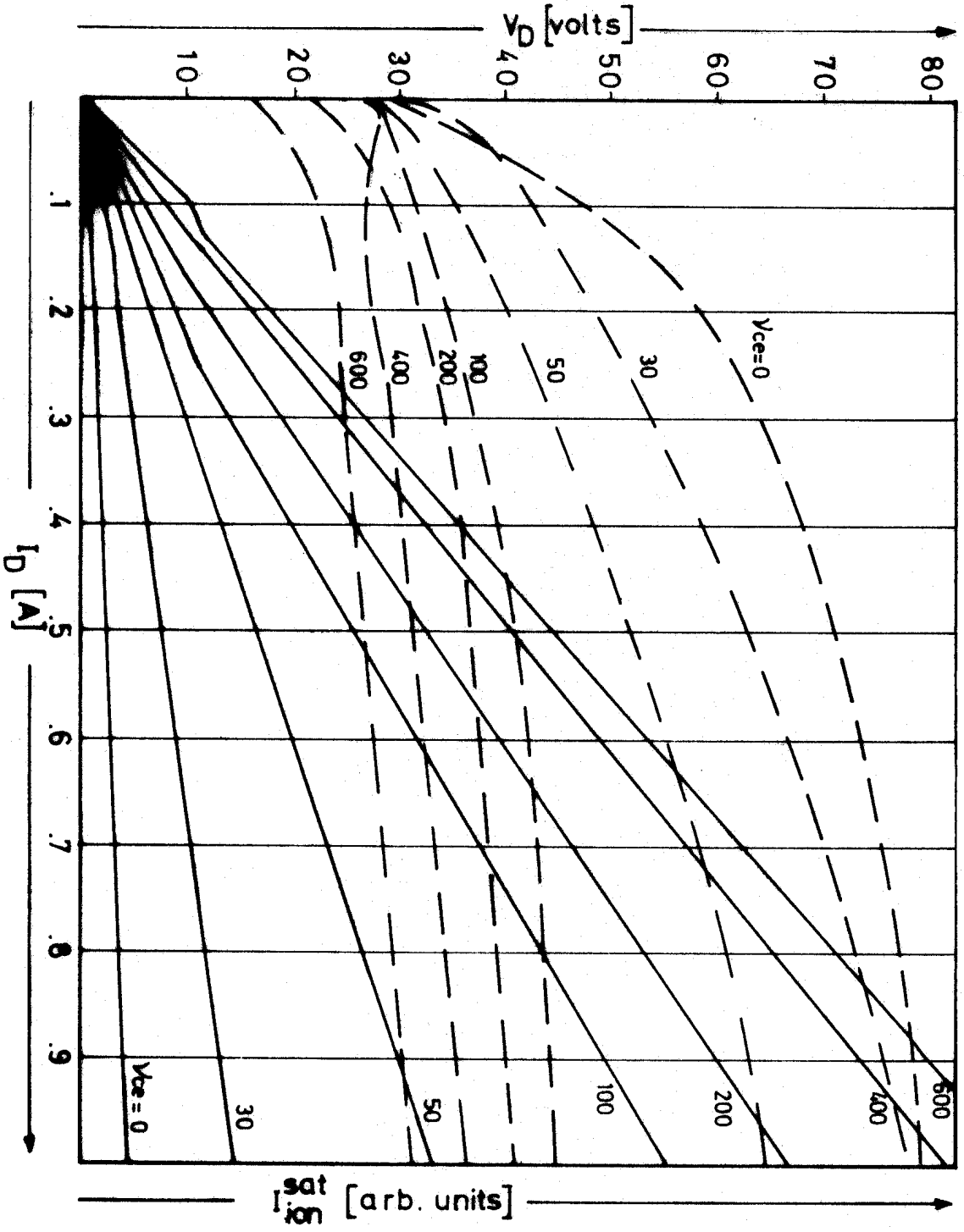
V_D [volts]
10
20
30
40
50
60
70
80
I_D [A]
.1
.2
.3
.4
.5
.6
.7
.8
.9
$V_{ce}=0$
30
50
100
200
400
600
I_{DS}^{sat} [arb. units]

Fig. 2

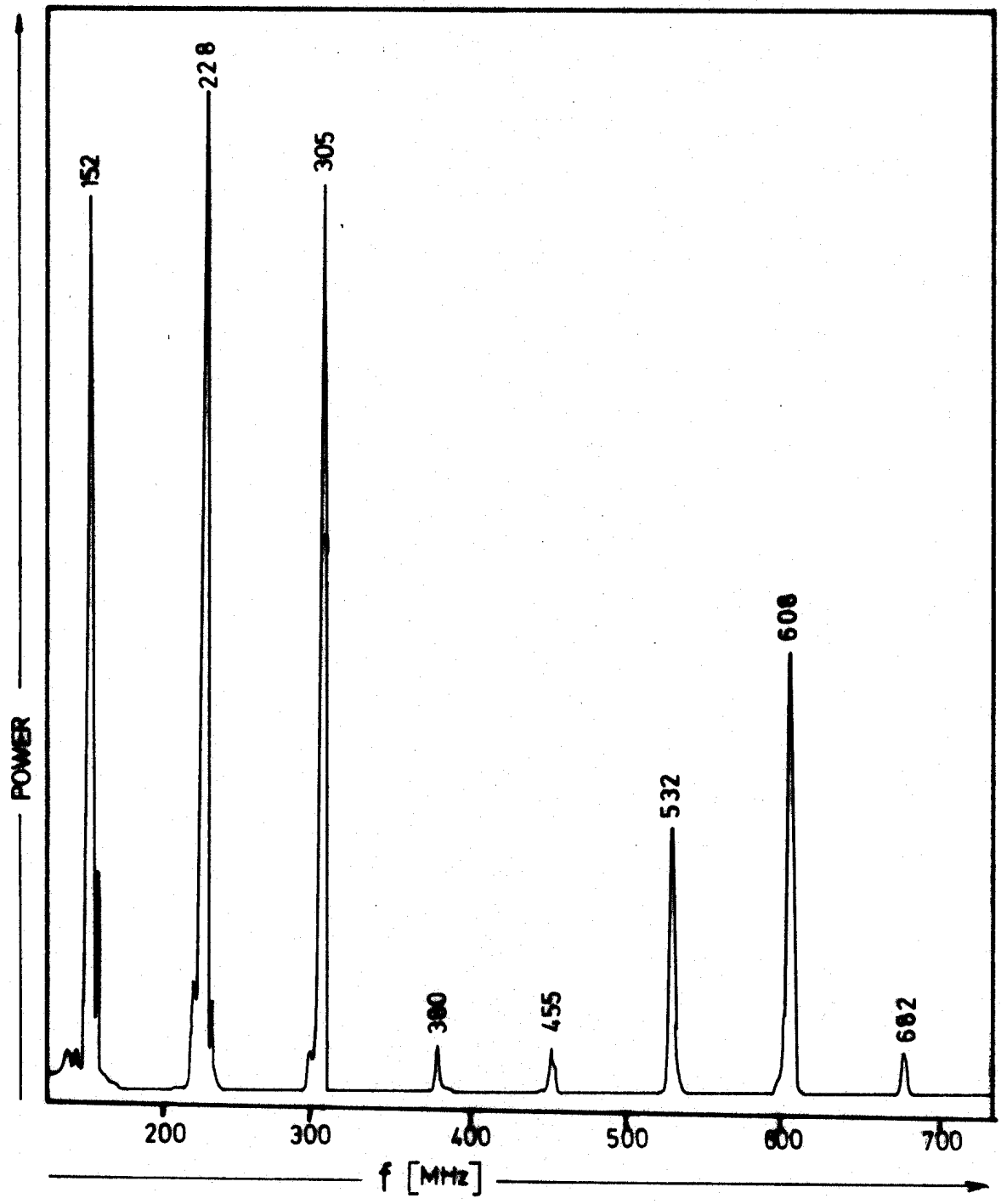
POWER
152
228
305
380
455
532
608
682
200
300
400
500
600
700
f [MHz]

Fig. 3

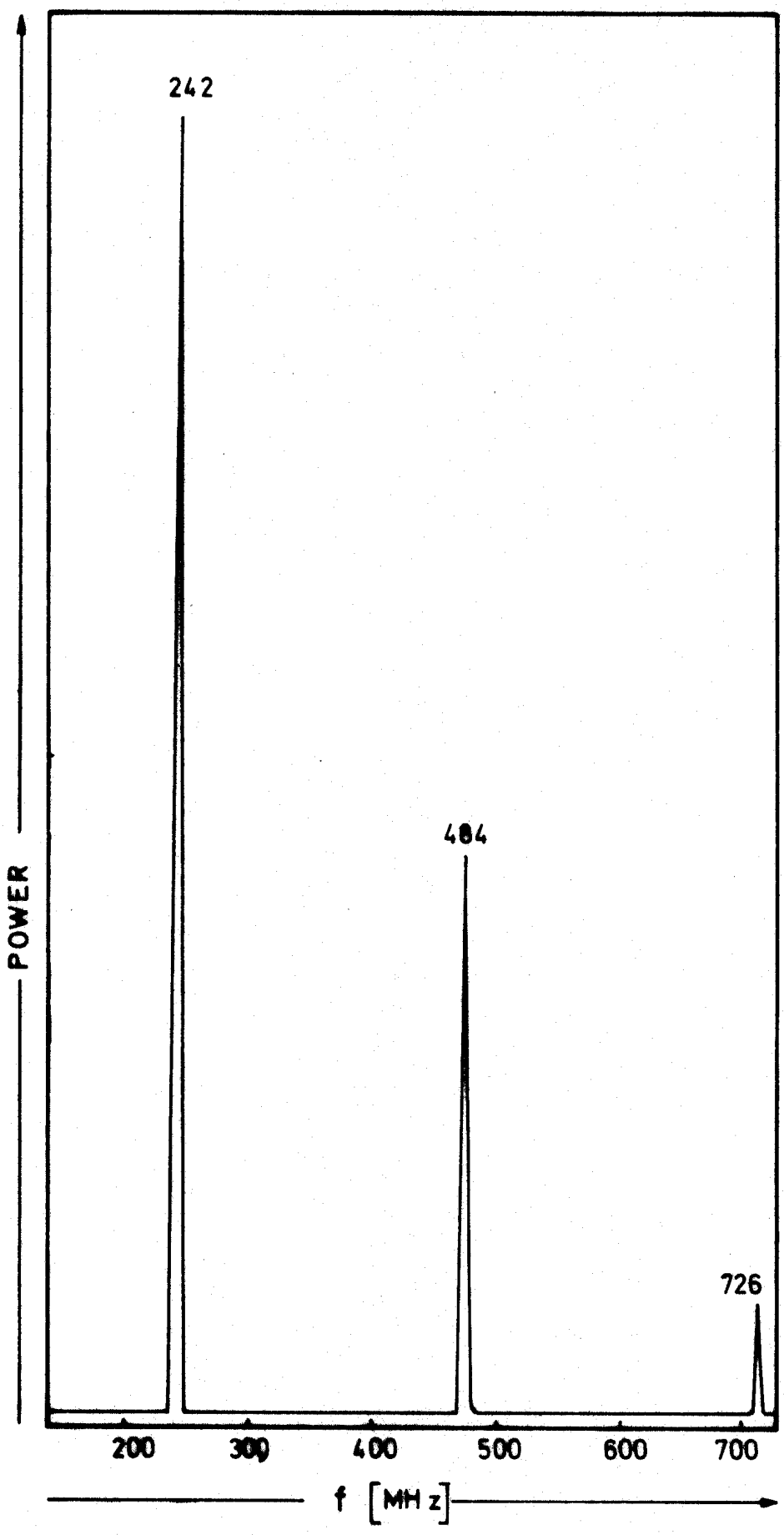

Fig. 4

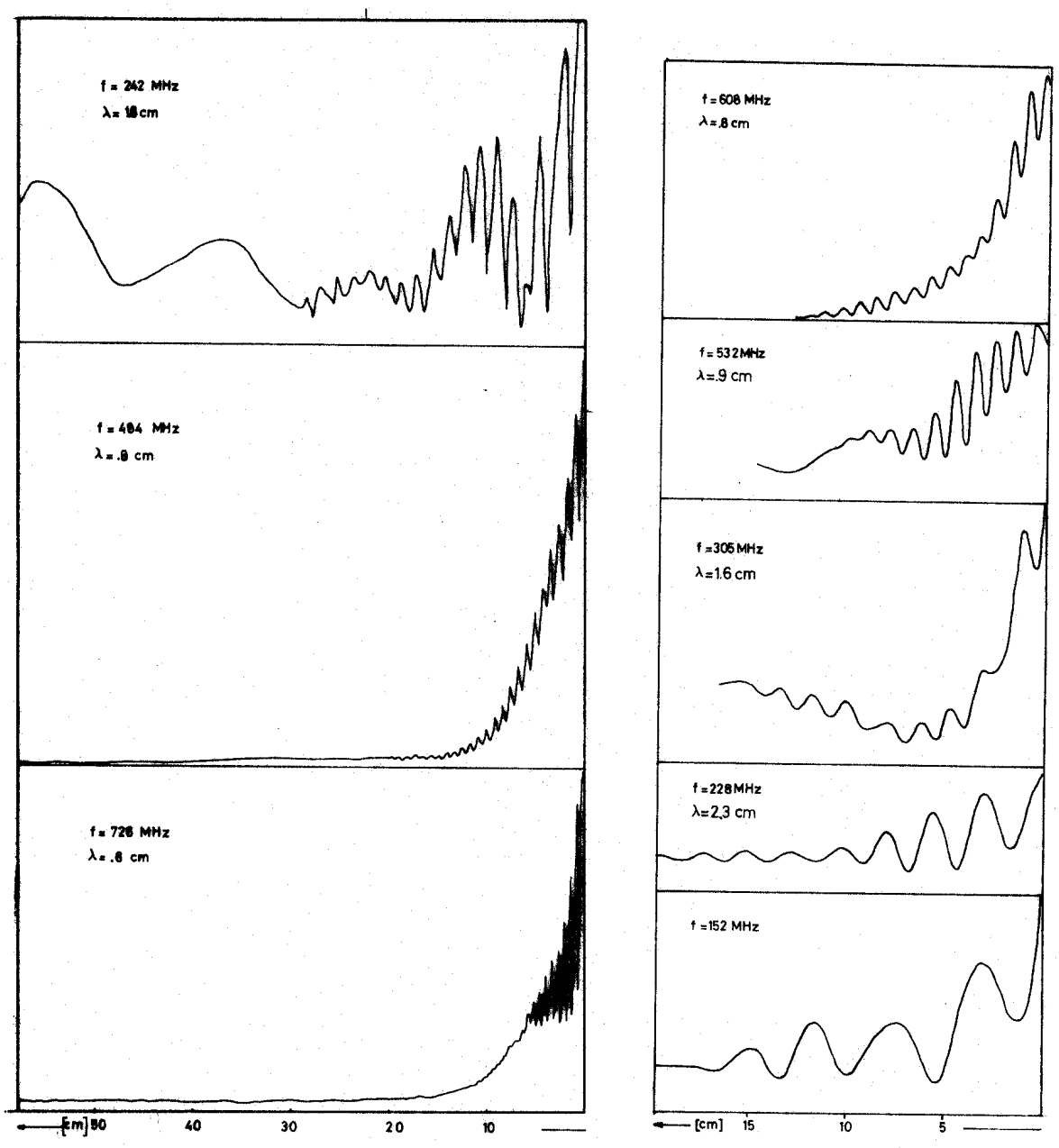
f = 242 MHz
λ= 18 cm
f = 484 MHz
λ = .9 cm
f = 726 MHz
λ = .6 cm
[cm] 50
40
30
20
10
f = 608 MHz
λ = .8 cm
f = 532 MHz
λ = .9 cm
f = 305 MHz
λ = 1.6 cm
f = 228 MHz
λ = 2,3 cm
f = 152 MHz
[cm] 15
10
5

(b) (a)

Fig. 5

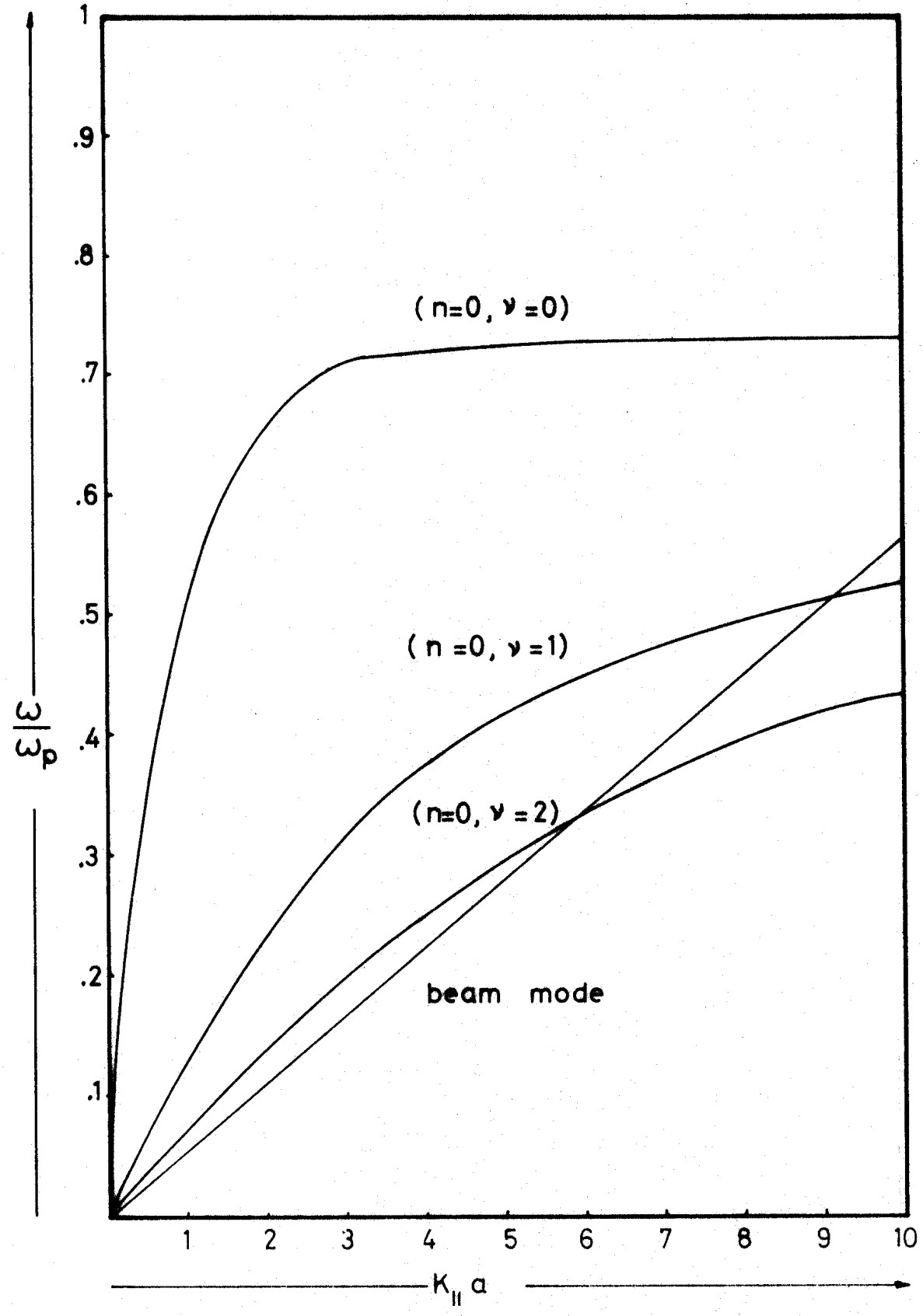

Fig.6

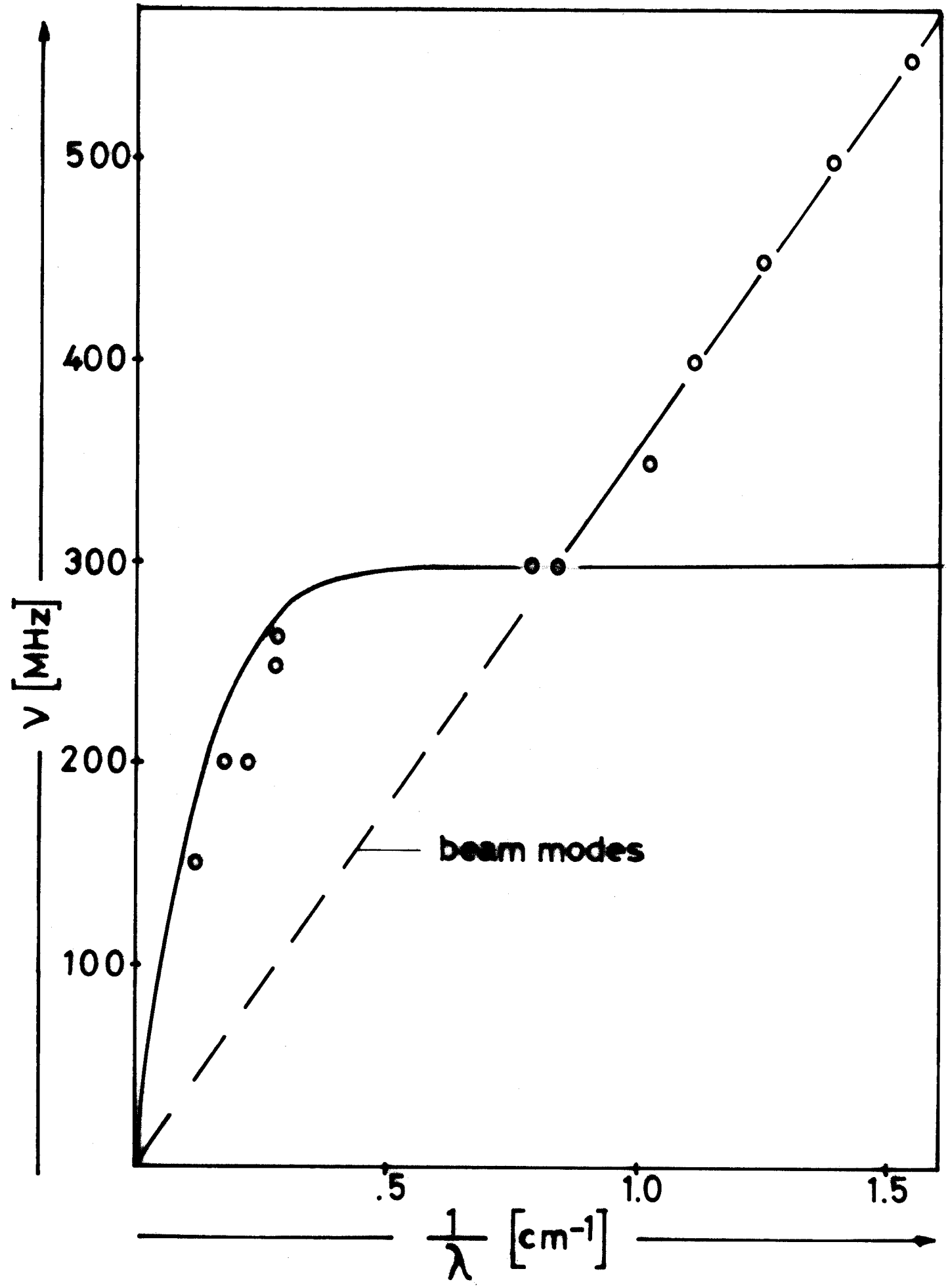

Fig. 2

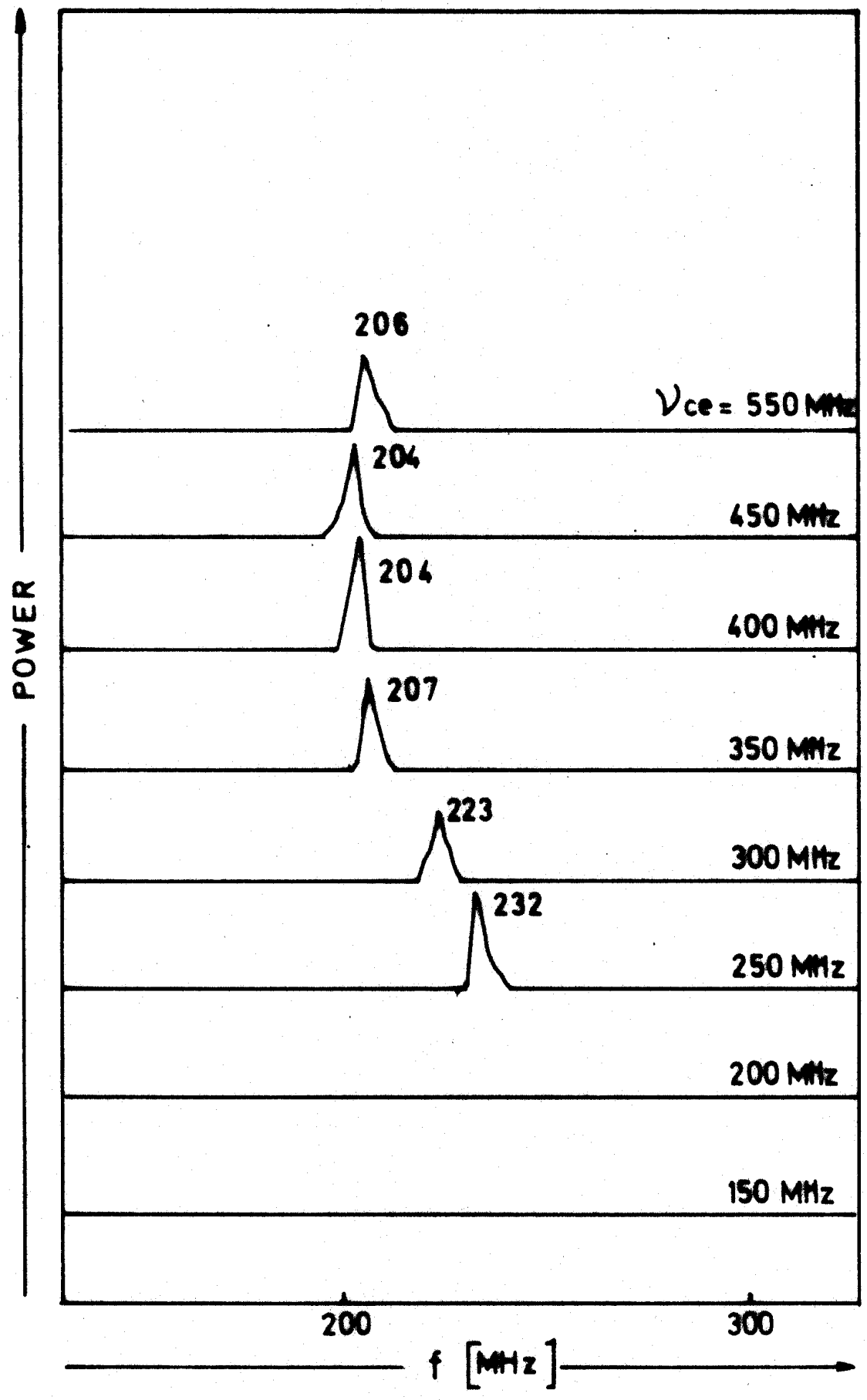
POWER
206
ν_{ce} = 550 MHz
204
450 MHz
204
400 MHz
207
350 MHz
223
300 MHz
232
250 MHz
200 MHz
150 MHz
200
300
f [MHz]

Fig. 8

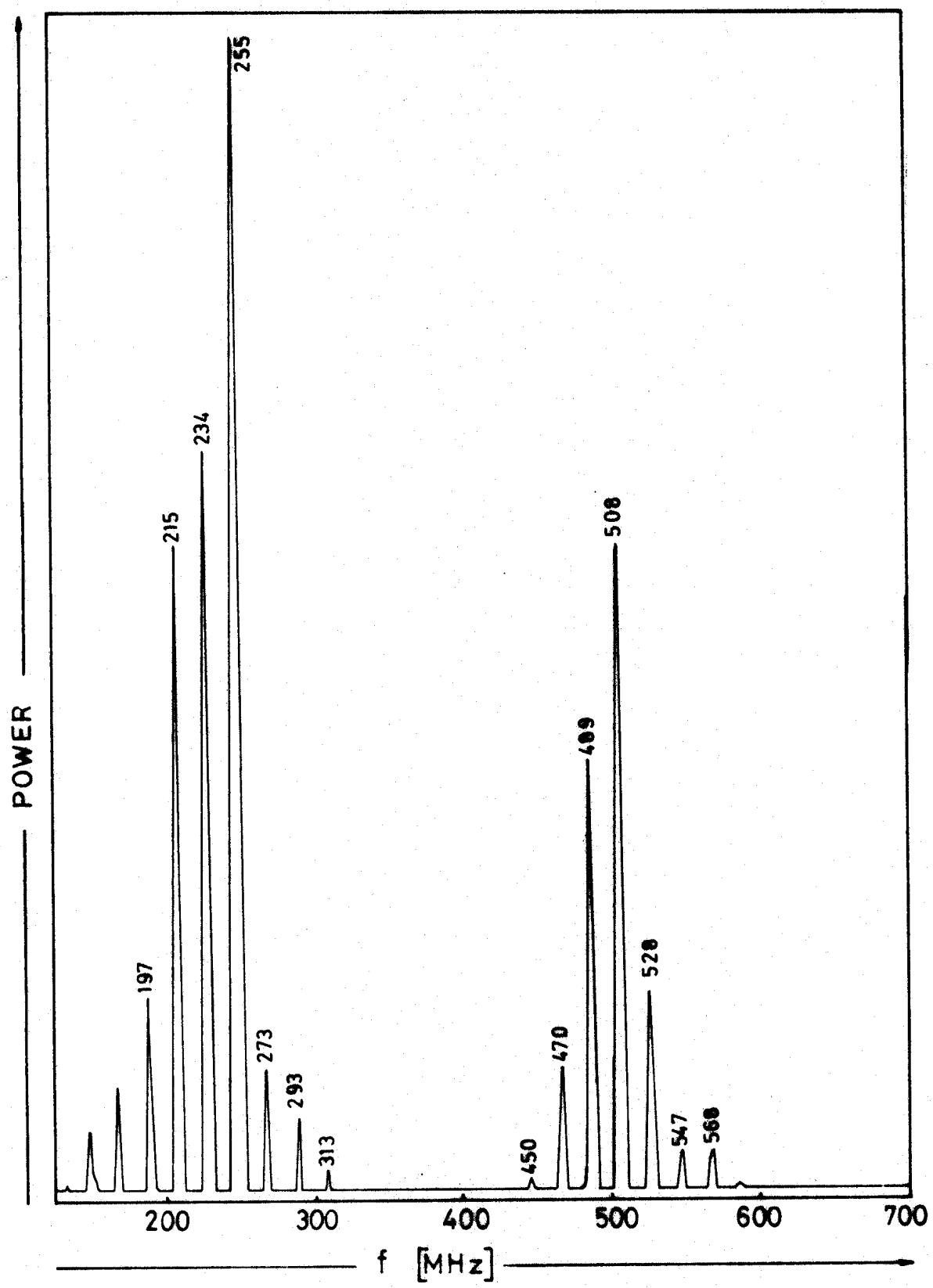
POWER
255
234
215
197
273
293
313
450
470
489
508
528
547
568
200
300
400
500
600
700
f [MHz]

Fig. 9

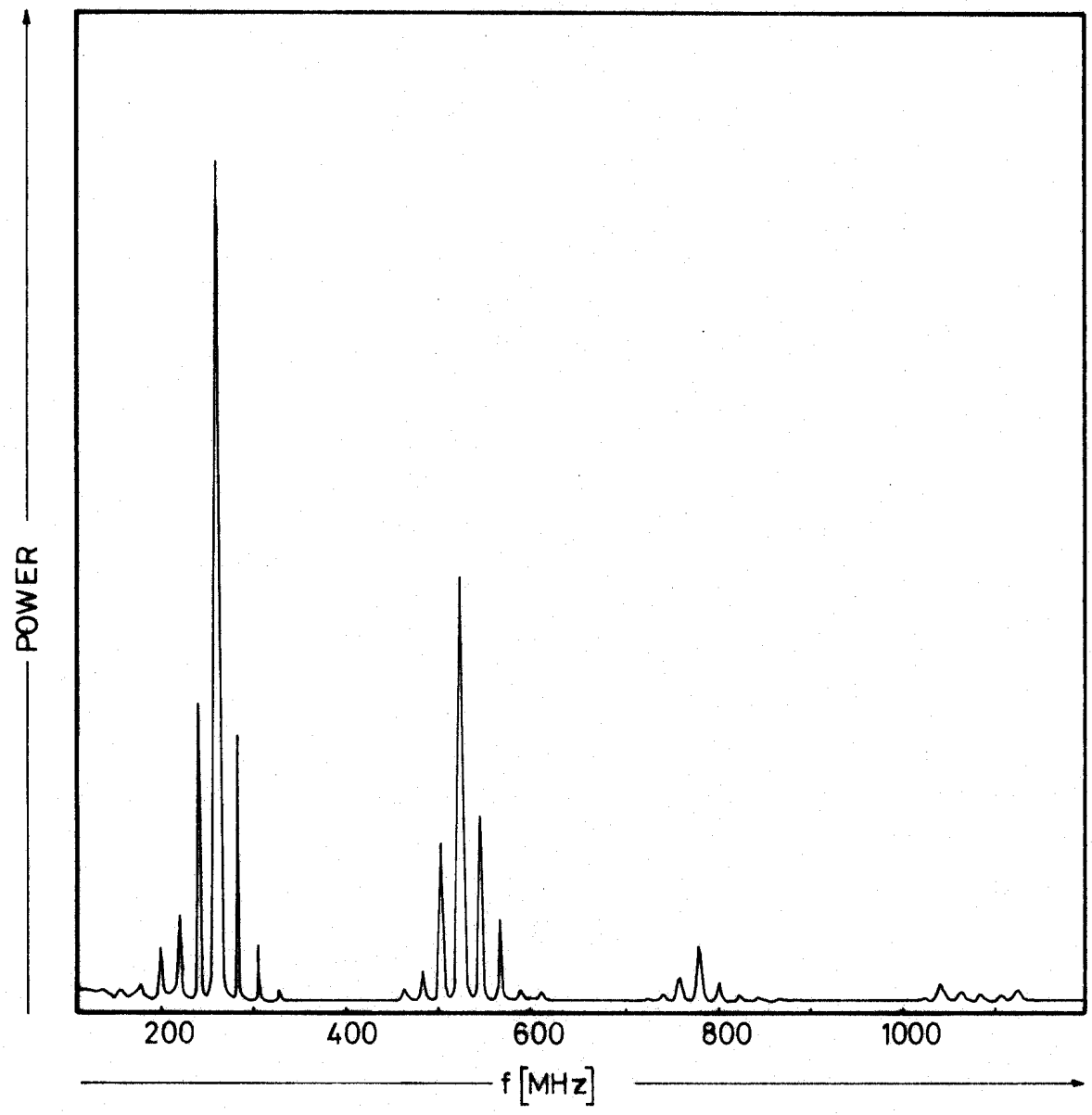

Fig. 10

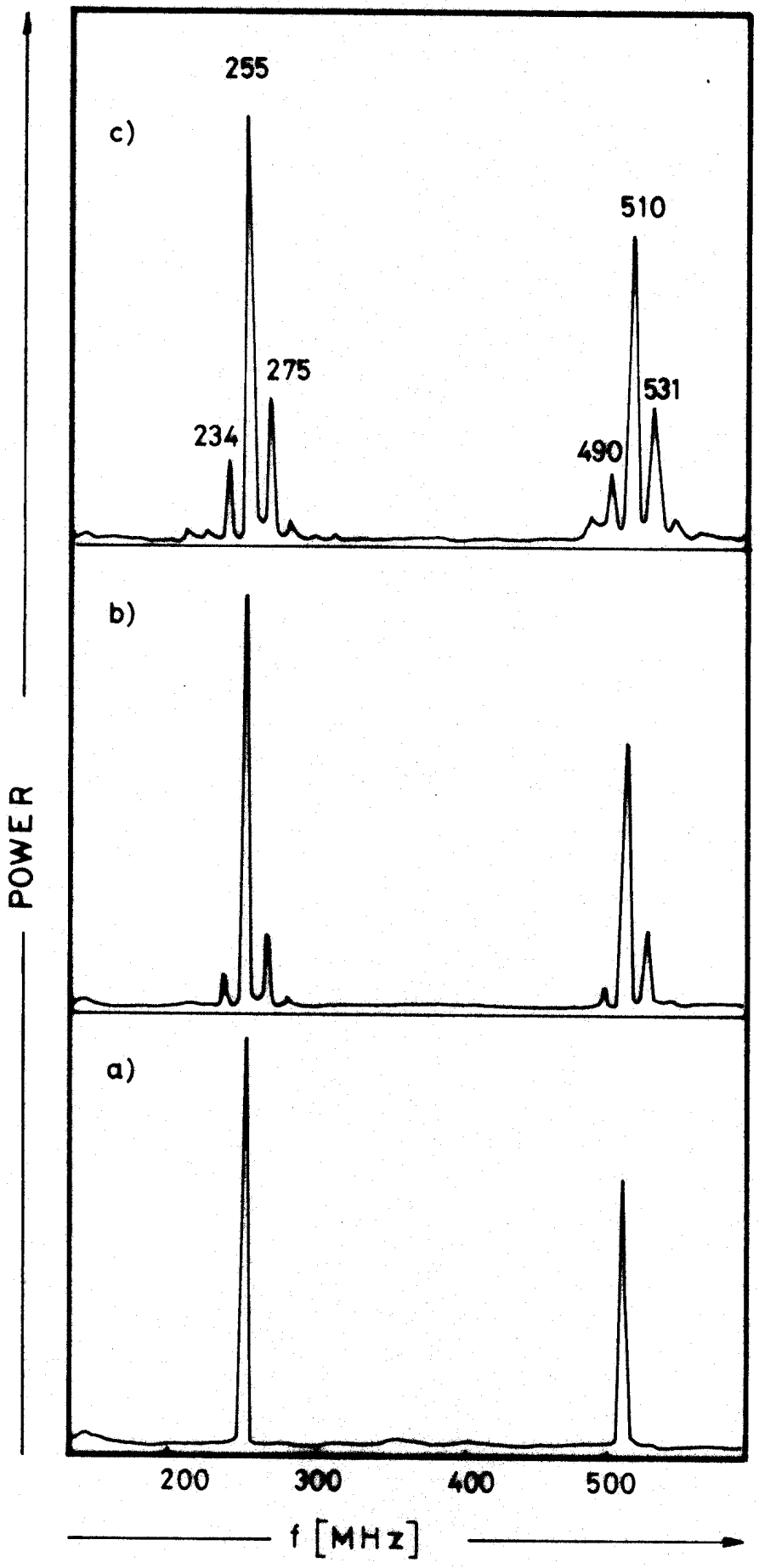

Fig. 11

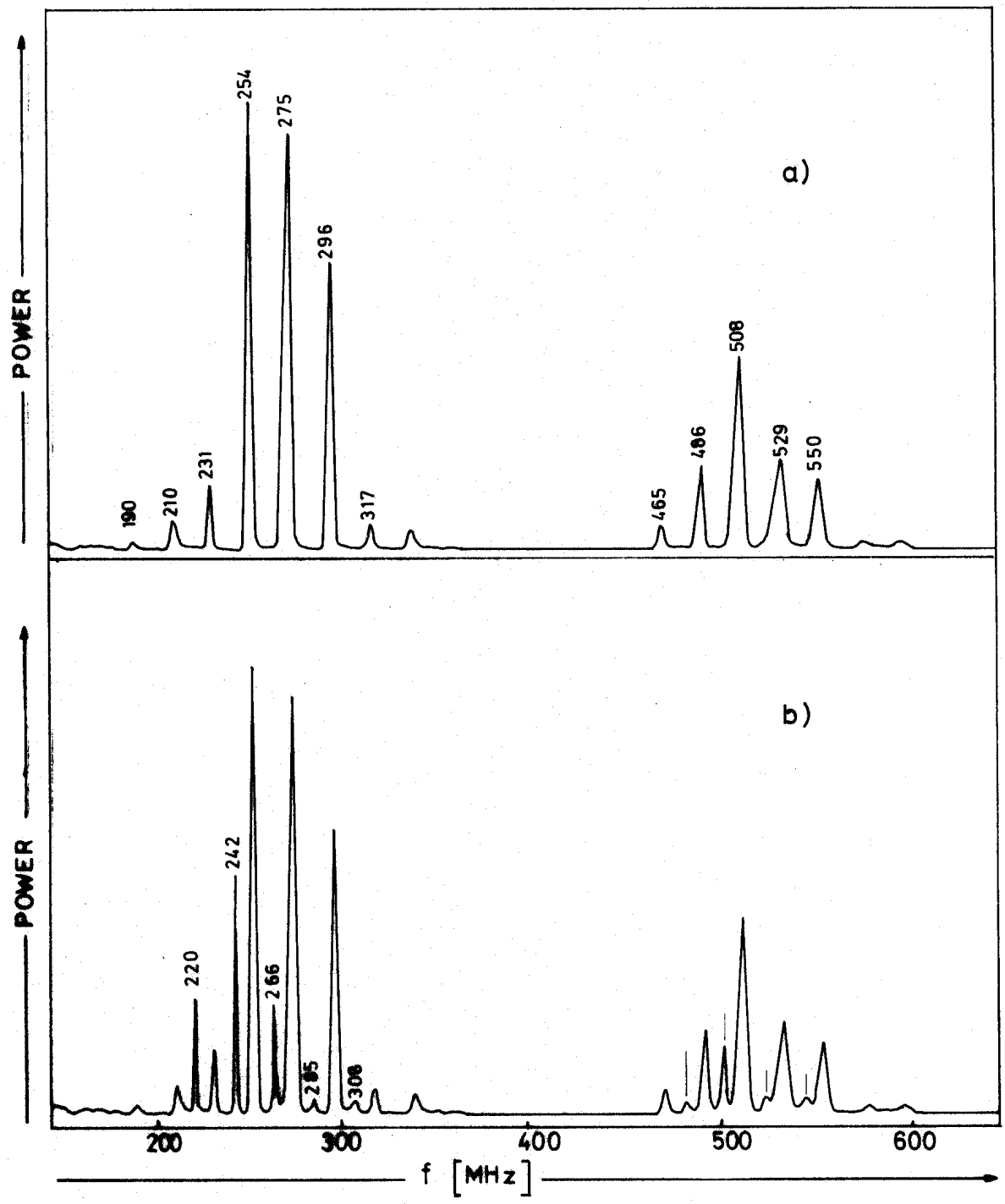
POWER
a)
254
275
296
190
210
231
317
465
486
508
529
550
POWER
b)
220
242
266
285
306
200
300
400
500
600
f [MHz]

Fig. 12